Naujoks, M., Kroner, C., Weise, A., Jahr, T., Krause, P., Eisner, S. (2010): Evaluating local hydrological modelling by temporal gravity observations and a gravimetric three-dimensional model. - Geophysical Journal International, 182, 1, pp. 233—249.

DOI: http://doi.org/10.1111/j.1365-246X.2010.04615.x

Geophysical Journal International

Geophys. J. Int. (2010) **182,** 233–249 doi: 10.1111/j.1365-246X.2010.04615.x

Evaluating local hydrological modelling by temporal gravity observations and a gravimetric three-dimensional model

M. Naujoks,[1] C. Kroner,[2] A. Weise,[1] T. Jahr,[1] P. Krause[3] and S. Eisner[4]

[1] *Institute of Geosciences, Friedrich-Schiller-University Jena, Burgweg* 11, D-07749 *Jena, Germany. E-mail: m.naujoks@uni-jena.de*
[2] *Helmholtz Centre Potsdam, German Research Centre for Geosciences, Telegrafenberg,* D-14473 *Potsdam, Germany*
[3] *Institute of Geography, Friedrich-Schiller-University Jena, Löbdergraben* 32, D-07743 *Jena, Germany*
[4] *Center for Environmental Systems Research, University of Kassel, Kurt-Wolters-Str.* 3, D-34109 *Kassel, Germany*

Accepted 2010 April 7. Received 2010 April 2; in original form 2009 August 5

SUMMARY

An approach for the evaluation of local hydrological modelling is presented: the deployment of temporal terrestrial gravity measurements and gravimetric 3-D modelling in addition to hydrological point observations. Of particular interest is to what extent such information can be used to improve the understanding of hydrological process dynamics and to evaluate hydrological models. Because temporal gravity data contain integral information about hydrological mass changes they can be considered as a valuable augmentation to traditional hydrological observations. On the other hand, hydrological effects need to be eliminated from high-quality gravity time-series because they interfere with small geodynamic signals. In areas with hilly topography and/or inhomogeneous subsoil, a simple reduction based on hydrological point measurements is usually not sufficient. For such situations, the underlying hydrological processes in the soil and the disaggregated bedrock need to be considered in their spatial and temporal dynamics to allow the development of a more sophisticated reduction.

Regarding these issues interdisciplinary research has been carried out in the surroundings of the Geodynamic Observatory Moxa, Germany. At Moxa, hydrologically induced gravity variations of several 10 nm s^{-2} are observed by the stationarily operating superconducting gravimeter and by spatially distributed and repeated high-precision measurements with transportable relative instruments. In addition, hydrological parameters are monitored which serve as input for a local hydrological catchment model for the area of about 2 km^2 around the observatory. From this model, spatial hydrological variations are gained in hourly time steps and included as density changes of the subsoil in a well-constrained gravimetric 3-D model to derive temporal modelled gravity variations.

The gravity variations obtained from this combined modelling correspond very well to the observed hydrological gravity changes for both, short period and seasonal signals. From the modelling the amplitude of the impact on gravity of hydrological changes occurring in different distances to the gravimeter location can be inferred. Possible modifications on the local hydrological model are discussed to further improve the quality of the model. Furthermore, a successful reduction of local hydrological effects in the superconducting gravimeter data is developed. After this reduction global seasonal fluctuations are unmasked which are in correspondence to GRACE observations and to global hydrological models.

Key words: Time-series analysis; Gravity anomalies and Earth structure; Time variable gravity; Hydrogeophysics; Hydrology.

1 INTRODUCTION

Time variable gravity observations are affected by every mass change occurring in the Earth's system based on Newton's law of gravitation (attraction) and deformations due to loading effects. Hence, gravity data contain integral information on not only tides, ocean loading, atmospheric mass redistributions and polar motion, but also on hydrology-related mass changes such as ground water table or soil moisture fluctuations. Both, local hydrological mass changes and large-scale variations have an impact on the gravity field.

The impact of hydrological variations, for example, from rain or snow, changes of the ground water table or the soil water content is observed in gravity data worldwide (e.g. Bonatz 1967; Lambert

& Beaumont 1977; Elstner & Kautzleben 1982; Mäkinen & Tattari 1988; Bower & Courtier 1998). In particular, the continuous high-resolution recordings of superconducting gravimeters show these broad-band effects in a range between a few nanometres per square second and 100 nm s^{-2} (10 nm s^{-2} = 1 μGal) (Peter *et al.* 1995; Crossley *et al.* 1998; Harnisch & Harnisch 1999; Imanishi 2000; Virtanen 2000; Kroner 2001; Zerbini *et al.* 2001; Amalvict *et al.* 2004; Abe *et al.* 2006; Neumeyer *et al.* 2006; Sato *et al.* 2006; Kroner *et al.* 2007).

From the hydrological point of view, this impact on gravity can be considered as a valuable data source because it provides a supplement to traditional meteorological and hydrological point observations. In this context, the questions arise to what extent the information from gravity data can be used to improve the understanding of hydrological process dynamics and to which potential the data provide for the parametrization and validation of hydrological models. One way to apply such data for hydrological model evaluation is the direct comparison between gravity variations and simulated storage changes computed with a hydrological model as described on a local scale by Hasan *et al.* (2006, 2008), Creutzfeldt *et al.* (2008) and Krause *et al.* (2009). A more sophisticated but also more promising way is presented in this paper: the conversion of simulated water storage variations to gravity changes using gravimetric modelling.

From the geophysical view point, hydrological variations represent a disturbing effect in gravity data, especially in high-resolution observations with superconducting gravimeters. As geodynamic signals like oscillations of the Earth's core or coseismic variations are expected in a similar or even smaller order of magnitude than hydrological variations, the gravity data require an *a priori* elimination of such an impact. Local hydrological fluctuations in particular have a crucial effect on gravity observations (Llubes *et al.* 2004; Boy & Hinderer 2006; Harnisch & Harnisch 2006; Imanishi *et al.* 2006; Kroner & Jahr 2006; Van Camp *et al.* 2006; Longuevergne *et al.* 2009). Meurers *et al.* (2007) show by modelling that the direct vicinity (<100 m) of the observatory at Vienna (Austria) has a substantial impact on the gravimeter signals for short period, transient variations caused by rainfall as well as for long-term hydrological changes. This is generally confirmed by Virtanen *et al.* (2006). By comparing local, regional and global hydrological models with gravity observations for the station Metsähovi (Finland) they conclude that about two-thirds of the observed hydrological variations of the signal are of local origin.

In general, the temporal and spatial complexity and variability of hydrological processes in the surroundings of a gravimeter make a quantification of the local hydrological effect in gravity data a challenging task. Previous investigations have been based on simplification of both geological context (e.g. homogeneous and horizontal layers in the subsoil) and hydrological process complexity. Because of such generalizations it is reasonably likely that local variations (1 km of vicinity) are only partially or inexactly captured. To avoid this, the local hydrological dynamics (Kroner & Jahr 2006; Hokkanen *et al.* 2007; Krause *et al.* 2009) must be considered in detail. We propose a combined detailed analysis of the local hydrological process complexity as well as the topographic and geological situation at the particular station.

For the first time terrestrial gravity observations are applied to reliably evaluate a hydrological model of a small catchment on the one hand, and to use the information of this local model to develop a reduction of local hydrological effects in superconducting gravimeter data on the other hand. These are the two central scientific aims of this paper.

2 OUTLINE AND METHODOLOGY

Interdisciplinary research has been carried out in the surroundings of the Geodynamic Observatory Moxa, Germany, comprising scientists from geophysics, hydrology, soil sciences and geology. The geological and hydrological situation around the observatory is described in Section 3. Variations in the Earth's gravity field are monitored at Moxa continuously with the stationarily operating superconducting gravimeter GWR CD034 for more than 10 yr showing a significant hydrological impact (Kroner 2001; Kroner *et al.* 2007). From repeated gravity measurements carried out with transportable LaCoste & Romberg (L&R) relative instruments on the local network MoxaNet (Naujoks *et al.* 2008) in the area around the observatory, spatial information on gravity changes were gained. They are used to constrain ambiguities, localize different hydrological compartments affecting gravity and separate the local hydrological effect from large-scale changes. The gravity observations are briefly introduced in Section 4.

A small-scale hydrological catchment model (Section 5) based on hydrological point observations and physio-geographical information was developed to study the hydrological processes in the surroundings of the observatory. Mass variations derived from the local hydrological model in hourly time steps were converted to density changes of the subsoil bodies of a well-constrained static gravimetric 3-D model, which was set up for the observatory surroundings (Sections 6 and 7). The output of this coupled hydrological and gravimetric modelling – temporal modelled gravity variations for the observation sites – is compared to the observed gravity changes (in Section 8 for the local network and in Section 9 for the superconducting gravimeter). Hereby, the temporal and spatial variability of hydrological variations in the gravity data is analysed. In this context the quality of the local hydrological model is evaluated leading to a proposal of possible modifications. Finally, the feasibility to develop a more sophisticated reduction of local hydrological effects in the superconducting gravimeter data is studied and some remarks on large-scale hydrological fluctuations are given. The principal approach of this study is illustrated in Fig. 1 which shows the three main study methods together with the major work tasks and the application of the results.

Moxa observatory with its vicinity (Jahr *et al.* 2001) is a well-suited location for these geophysical and hydrological investigations because its noise level from the tides to the seismic band (10^{-5} to 5 mHz) is one of the lowest worldwide (Kroner *et al.* 2004; Rosat *et al.* 2004), numerous hydro-meteorological parameters are observed, the geology of the subsoil is well investigated (Kasch 2006) and a number of hydrological investigations have been carried out (Hasan *et al.* 2006, 2008; Kroner & Jahr 2006; Krause *et al.* 2009). Besides this, many geoscientific boundary conditions from geophysical surveys are available and contribute directly to well-constrained hydrological and gravimetric modelling of the complex hydrological situation at Moxa observatory.

3 GEOLOGICAL AND HYDROLOGICAL SITUATION AT MOXA OBSERVATORY

The Geodynamic Observatory Moxa is located 30 km south of the city Jena (Thuringia, Germany) in the headwater catchment of the creek Silberleite that covers an area of approximately 2 km^2 with elevations between 450 and 540 m above mean sea level. Nearly the whole catchment is covered by coniferous forest. Only very small parts in the west and east of the observatory are used for agricultural purposes.

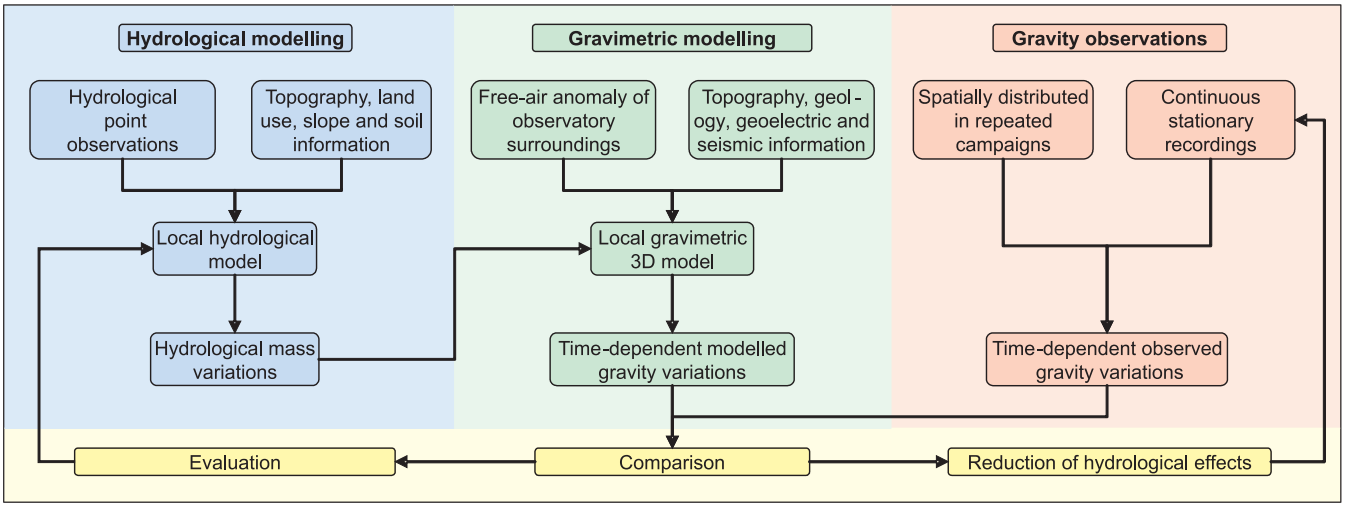

Figure 1. Flow chart illustrating the combination of local hydrological modelling, local gravimetric modelling and the gravity observations at Moxa.

The geological underground consists of folded series of crystalline schist and greywacke of the Lower Carboniferous (Kasch 2006). The bedrock is very compact but has a strongly fractured top layer. The fractures are mostly oriented vertically resulting in preferential flow paths for fast infiltration of subsurface water. The soil types around the observatory were mapped in a field campaign resulting in a soil map (Scholten *et al.* 2004) which is based on more than 30 soil profiles. The soils are mostly cambisols with a partially significant clay fraction and a considerable rock fraction of about 30 per cent in the middle horizons and more than 70 per cent in the lower horizons. At the valley bottom, ground water-influenced soils (gleysol) can be found. Cambisol in the forest and gleysol at the valley bottom provide a hydrologically unsaturated and very permeable water storage with weathering/decomposition layer. It is underlain by strongly jointed as well as partially faulted and weathered rock (disaggregated bedrock).

The meteorological parameters temperature, precipitation, illuminance, wind speed and direction and relative humidity are monitored at the observatory every 10 s. Barometric pressure changes are recorded every second. The climate is humid with a mean annual temperature of 7.7 °C based on the years from 2000 to 2006, a mean annual rainfall of 733 mm, and an actual evapotranspiration of 524 mm which was estimated using the equation of Penman–Monteith (Monteith 1975) and applying a reduction function for soil water stress (Krause 2001).

The east–west profile of the Silberleite valley (Fig. 2) illustrates the topographic and hydrological situation and the main hydrological processes in the immediate observatory vicinity. Because of the specific topographic situation the water can be stored above and below the level of the gravity observation sites in the form of interception, soil moisture, snow and ground water. Short-, middle- and long-term storage capacities for the water are provided by the canopy, the disaggregated bedrock, the soil matrix and the ground water aquifer. During winter, water storage in the form of snow occurs. Directly to the east of the observatory building a steep slope is located which was identified as a gravimetrically significant hydrological compartment (Kroner & Jahr 2006; Naujoks *et al.* 2008). Rainwater on this slope is mainly generating interflow with a quick response time of only a few hours.

Hydrological research and modelling at the test site in Moxa (Hasan *et al.* 2006, 2008; Kroner *et al.* 2007; Krause *et al.* 2009) confirmed that the gravimeter signal shows variations which are correlated to various hydrological processes like rainfall, snow accumulation and melt, soil moisture changes and changes in the water table. The impact of such hydrological changes on the gravity measurements has only been roughly investigated yet, because the time variable mass changes all over the area are complicated due to the inhomogeneous subsoil, topographic changes and flow processes.

4 GRAVITY OBSERVATIONS

4.1 Continuous recordings with the superconducting gravimeter

The superconducting gravimeter at Moxa observatory is part of the Global Geodynamics Project (GGP) (Crossley *et al.* 1999) in which variations of the Earth's gravity field are monitored with an accuracy of better than 1 nm s^{-2} in the time domain (Kroner *et al.* 2004; Rosat *et al.* 2004). The gravimeter signal is affected by various effects. Earth and ocean tides, non-tidal oceanic loading (Kroner *et al.* 2009), atmospheric mass redistributions (Neumeyer *et al.* 2007; Abe *et al.* 2010), polar motion and instrumental drift are eliminated from the data resulting in the residual time-series which contains hydrology-induced gravity variations as main remaining signals.

Significant effects due to hydrology in an order of magnitude of some 10 nm s^{-2} could be proved by Kroner (2001) and Kroner *et al.* (2004, 2007). In particular, an anticorrelation between gravity and the hydrological situation is observed, caused by specific topographic conditions (Fig. 2). Because the observatory is built close to a steep slope, most of the hydrological variations in the near vicinity occur above gravimeter level. During rain events with successive high water table and soil moisture in the gravimeter surroundings, water mass is first stored above the gravimeter level, leading to a fast gravity decrease. In the hours and days after the rain event a successive gravity increase is observed caused by both water moving downwards below the gravimeter level and evaporating rainwater that was intercepted by vegetation or retained by the soil.

4.2 Repeated measurements with L&R gravimeters on the local network MoxaNet

Local hydrology models are typically calibrated by hydrological and meteorological measurements. From observations of a

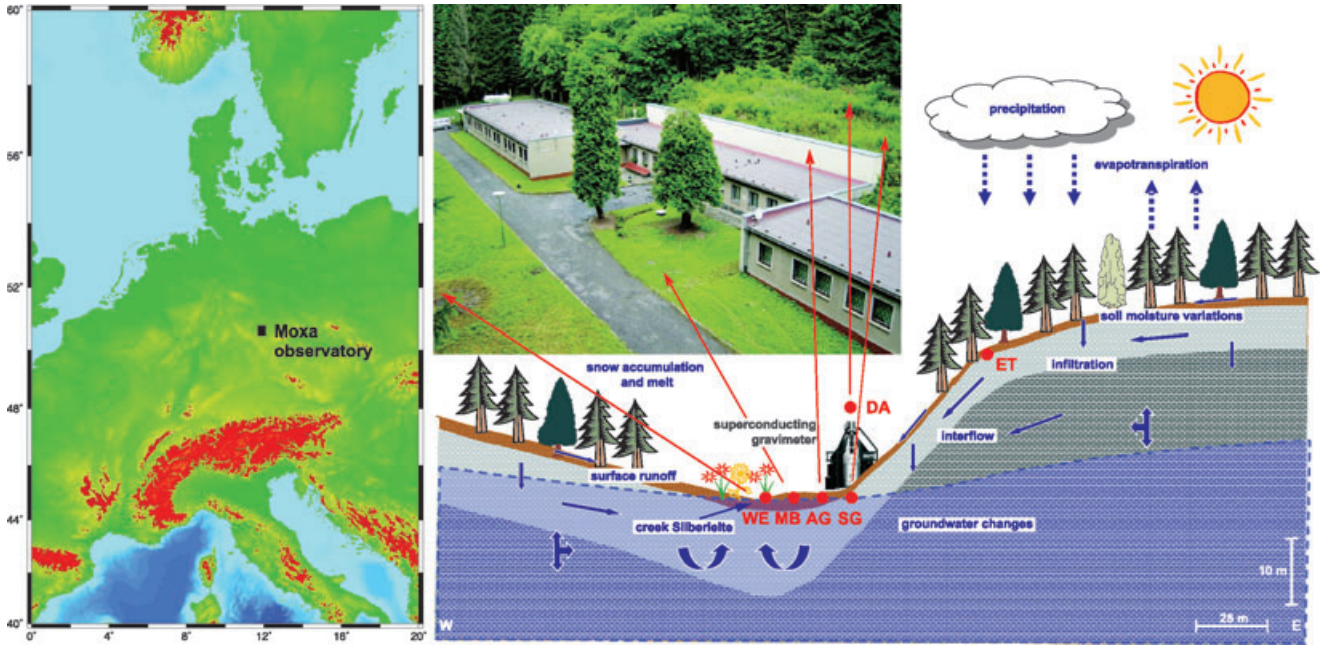

Figure 2. Left-hand side: location of Moxa observatory in Europe; Right-hand side: sketch of the hydrological processes and flow paths at Moxa observatory, and location of the superconducting gravimeter and the observation points in the local gravity network MoxaNet (red points, Section 4.2).

superconducting gravimeter an additional calibration is possible to a certain extent. However, the instrument captures the integral signal of both local and large-scale hydrological effects, which usually can only be separated by very precise and spatially distributed repeated measurements of gravity differences on a local network. Mäkinen & Tattari (1991) showed that a measured gravity difference can significantly change by local hydrology-related variations. Such measurements hold the potential to localize areas with a considerable hydrological influence on gravity (e.g. Merlet *et al.* 2008; Jacob *et al.* 2009). In the repeated difference measurements only local changes are observed because large-scale fluctuations have the same impact at both points and cancel each other out in the difference. Thus, these measurements are particularly suited to evaluate a local hydrological model. They give a unique opportunity to quantify the local hydrological influence and separate it from the large-scale changes.

For this purpose, the local gravity network MoxaNet was established in the vicinity of Moxa observatory (Naujoks 2008; Naujoks *et al.* 2008). The network runs roughly east–west perpendicular to the Silberleite valley (Fig. 2). It consists of six observation sites in distances from a few up to 65 m from each other in hydrologically different areas. The point ET is situated on the hill to the east of the observatory near the top of the steep slope, and the point DA on the observatory roof. Another point SG is located next to the superconducting gravimeter in the observatory building at the base of the steep slope. Three more sites (AG, MB and WE) are situated in the valley in increasing distances to the superconducting gravimeter. The point AG is located inside the observatory building, the points MB and WE outside and the point WE next to the Silberleite creek in an almost permanent saturated area.

5 LOCAL HYDROLOGICAL MODELLING

For the hydrological modelling of the Silberleite catchment the fully distributed process-oriented hydrological model J2000 was used (Krause 2001; Krause *et al.* 2009). Applying the model, good results were obtained for different catchments (e.g. Krause 2001; Krause *et al.* 2006). J2000 implements the hydrological processes evapotranspiration, snow accumulation and melt, interception, infiltration and soil water movement and ground water recharge as conceptual approaches. For the modelling, the climate data precipitation, temperature, illuminance, relative humidity and wind speed, measured at the observatory, were used as driving forces.

The Silberleite catchment with an area of about 2 km^2 (Fig. 3) was partitioned into 337 process-oriented response areas—hydrological response units (HRUs)—which were delineated according to the relevant physio-geographical input information (topography, landuse, soil types and geology). Each HRU is represented by different water storages (surface depression storage, snow storage, interception storage, soil storage and ground water storages) which interact with each other and show an areal variability (Krause *et al.* 2009). Lateral water movement from one unit to the next is simulated by topological connections between the single units (Fig. 3). Based on these connections, flow cascades are implemented which route the flow components (overland flow, interflow and quick and slow baseflow) through the units and finally into the creek, following the maximum topographic gradient. Inside the creek, the water is routed as streamflow to the catchment outlet. A detailed model description is given in Krause (2001) and Krause *et al.* (2006). The model was applied in hourly time steps for the period from 2003 October 23 to 2007 May 27. It was calibrated with the observed streamflow records and validated against *in situ* soil moisture measurements (Krause *et al.* 2009).

From the comparison of the simulated to the observed streamflow values near the observatory (Fig. 4) emerges that the hydrological dynamics could be reproduced fairly well. The catchment is characterized by higher flows during winter and in particular during snow melt events in spring, whereas in summer the streamflow is in general low with some single flood events, for example, in 2006 August. However, some small peaks in summer are not fully reproduced. They are caused by convective summer rainfalls, which

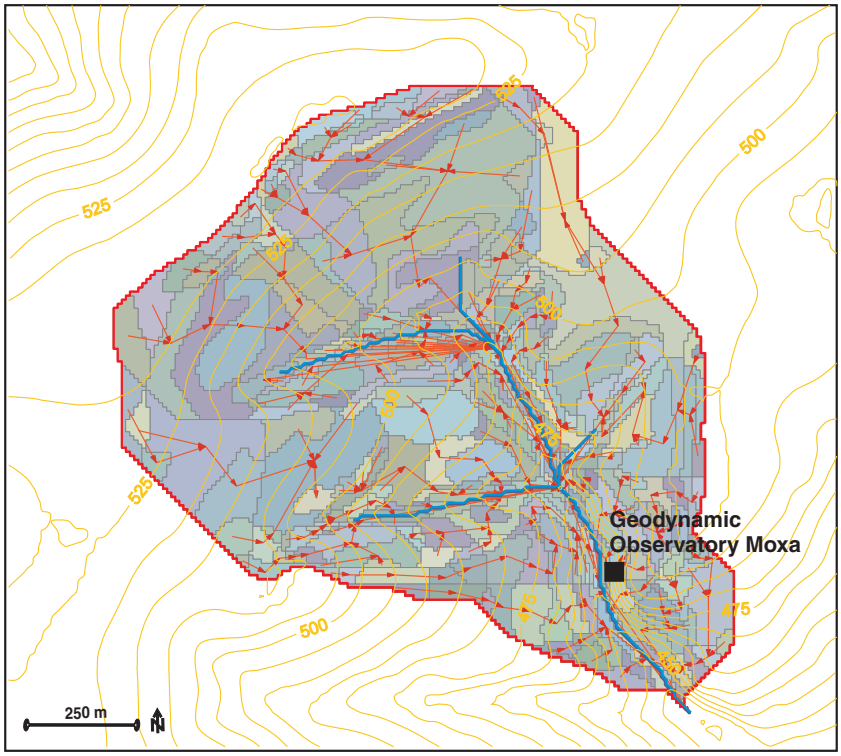

Figure 3. HRUs of the hydrological model of the catchment of the creek Silberleite (blue line) and lateral routing of the water between the HRUs to the creek following the maximum topographic gradient (red arrows).

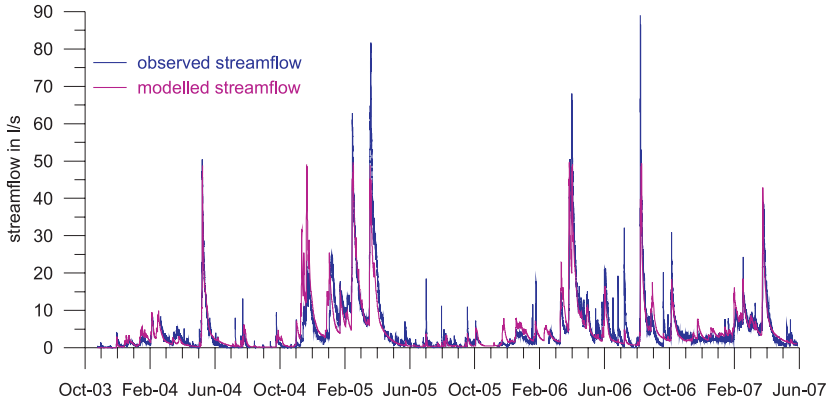

Figure 4. Observed and modelled streamflow of the creek Silberleite at the weir at the observatory representing the quality of the hydrological model.

are short-term but have high intensities. In these situations, rainfall intensity may exceed the infiltration capacity of the soil, leading to infiltration excess overland flow. The hydrological model was run with hourly time steps while these events may occur on smaller timescales. Thus, these peaks are not simulated correctly. The mismatch between modelled and observed peakflows results in a rms error of 4.11 $l\,s^{-1}$. On the other hand the Nash–Sutcliffe efficiency value of 0.8 (Nash & Sutcliffe 1970) and the relative volume error of 0.61 per cent confirm that the model is generally able to reproduce the hydrological variability of the catchment.

For the combination of the hydrological with a gravimetric model (Section 6), the actual contents of all storages of each HRU and time step were read out by J2000. In Fig. 5 the spatially averaged storage contents of all HRUs for the modelling period is given. The medium pore storage which represents the useable field capacity of the catchment is the most important one in terms of water storage. The storage contents visualize the high temporal dynamics of the hydrological state variables. The surface depression and the large pore soil storage show an immediate reaction on rain events (*cf.* Fig. 4) followed by a quick decay. Such quick reaction can also be observed for the quick ground water storage. The variations of the medium pore storage are more attenuated and show a clear seasonality as of course the snow storage does as well. This seasonality is even more pronounced in the curve of the total sum of all storages (red line in Fig. 5).

6 GRAVIMETRIC THREE-DIMENSIONAL MODELLING

To compute gravity changes from the hydrological mass variations derived from the hydrological model, a 3-D gravimetric model of the area around Moxa observatory was set up utilizing the

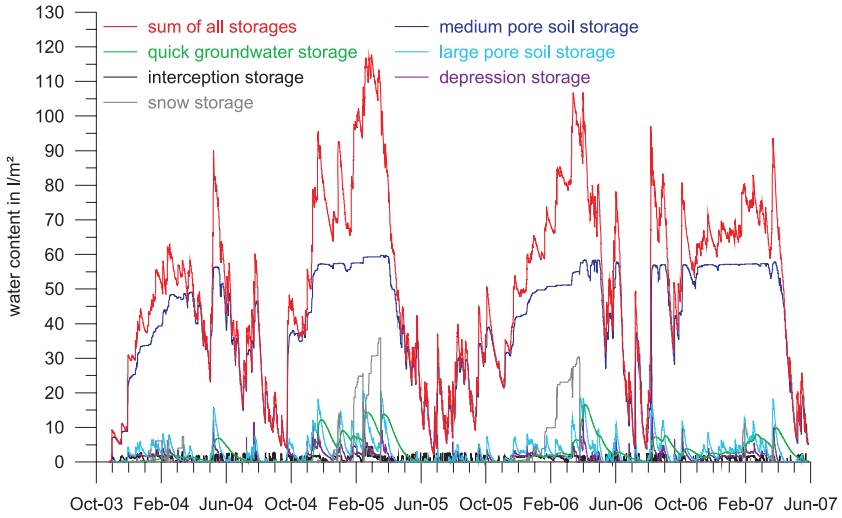

Figure 5. Mean water content of all hydrological mass storages, spatially averaged over all HRUs.

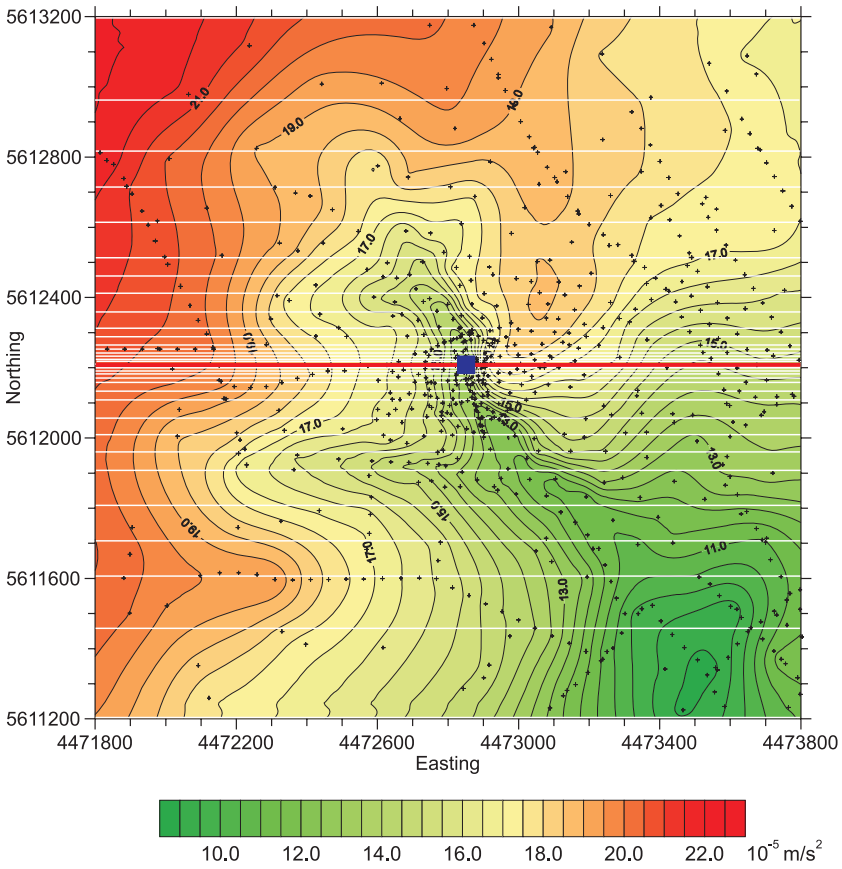

Figure 6. Gravimetric points (black crosses) and free-air anomaly in the surroundings of Moxa observatory. The 38 vertical planes of the gravimetric 3-D model (white lines) are included. Plane 19 running through the observatory (blue square) is marked in red (*cf.* Fig. 7).

software package Interactive Gravity and Magnetic Application system (IGMAS, Götze 1976, 1984; Götze & Lahmeyer 1988; Schmidt 1996, 2000).

6.1 Data base and free-air anomaly

In a first step a gravity anomaly map of the surroundings of Moxa observatory was compiled to provide a basis for the gravimetric modelling. According to the distance dependency of gravity and the natural features namely the topography and the local geology, a gravimetric survey area of 2 × 2 km^2 around the superconducting gravimeter was selected. Gravity measurements with L&R gravimeters were carried out at 460 locations (Fig. 6). For each location the position, the elevation and the surrounding topography up to a distance of 200 m were also determined.

To reach a high resolution in the modelling of local geological and hydrological structures in the close vicinity of the observatory a very high resolution of the gravity anomaly is required in the

Table 1. Thickness of the soil and the disaggregated bedrock around Moxa observatory (soil layer in the Silberleite valley inclusive artificial valley fill).

Thickness (m)	Soil	Disaggregated bedrock
In the valley	2.4–4.0	13–18
Steep slope east of observatory	0.2–0.5	3.5–5
Plateau around Silberleite valley	1.3–2.3	9–12

immediate surroundings of the observatory. To allow for this, a maximum distance of 5–10 m between the points was chosen in this area. With increasing distance from the observatory the point distance was increased stepwise to 25, 50, 100 and, finally, 150 m. With the large number and high density of gravity points a very good databasis for a small-scale 3-D gravimetric modelling of the subsoil was provided. Taking into account also any reductions applied to the measured data, an accuracy of the resulting free-air anomaly (Fig. 6) of about 0.04×10^{-5} m s^{-2} (1×10^{-5} m s$^{-2} = 1$ mGal) was gained. The free-air anomaly served as base for the modelling of the density structure of the subsoil reflecting the hilly topography (Fig. 3) and covering a gravity range of 14×10^{-5} m s^{-2} with lower values in the valley at and south of the observatory, but higher values on the plain northwest of the observatory.

6.2 Boundary conditions

To limit the ambiguities that are associated with potential methods and ensure a realistic modelling, the inclusion of extensive geological, tectonical and geophysical constraints in the gravimetric model was required. The wavelengths and amplitudes of the folded geological layers result from a geological mapping and a geological/tectonical model (Kasch 2006). They were directly used for the gravimetric modelling. Further constraints, in particular regarding the type and the thickness of the soil and the aquifereous layer of disaggregated bedrock, were derived from the soil map of Scholten *et al.* (2004) as well as from digging and drilling in the observatory gallery and its surroundings. Results from small-scale seismic and geoelectric measurements provide spatial information on the thickness of the soil and the disaggregated bedrock (Table 1). The densities of the soil layers were determined *in situ*, the densities of the disaggregated and the intact bedrock in the laboratory. Additionally, pore volumes of up to 30 volumes per cent were determined for the soil in depths up to 1 m.

6.3 The 3-D model

A sufficiently precise implementation of the topography and the soil layers is important to correctly represent the hydrological situation. For the modelling the area was divided into 38 vertical planes (Fig. 6). The essential topographical, hydrological and geological details were included into the model in high resolution. To avoid edge effects, the lateral extension of the model planes exceeds the area of gravity calculation by 10 km. The planes were oriented east–west, perpendicular to the valley of the creek Silberleite. The planes in the immediate surroundings of the observatory were chosen with a very small distance of 5 m (Fig. 6) resulting in a very high resolution of few metres for the topography as well as for hydrologically relevant structures. With increasing distance to the observatory, the distance between the planes was increased gradually up to 150 m (Fig. 6). Within the planes polygons (lines) characterize the geological model bodies. Between the planes, the polygons are connected by triangulation and build up 3-D bodies, to which a density value is assigned. The gravity effect of these 3-D bodies was calculated and compared to the observed free-air anomaly. By iterative variation of the model parameters (geometry and density of the bodies) the modelled gravity is approximated to the observed free-air anomaly to ensure a gravimetric modelling close to reality for the further investigations.

In Fig. 7 plane 19 of the gravimetric 3-D model is shown which runs directly through the observatory (*cf.* Fig. 6). In the upper part the observed free-air anomaly is given in red. The calculated anomaly, dotted in black, results from the topography and the density model in the lower part of the figure. Besides the bedrock, two layers were added to the model: a soil layer, consisting of cambisol in the forest and gleysol in the floodplain and a layer of disaggregated bedrock for each geological unit. In Fig. 8 the entire gravimetric 3-D model is given including the disaggregated and intact bedrock of the particular geological unit as well as gleysol in green and cambisol in yellow as soil layer. Up to a distance of 250 m from the observatory the soil layer and the disaggregated bedrock were divided into the respective HRUs of the local hydrological model. The triangulation of the surface on the topography and of the geological layers between the planes of the 3-D model is also included in Fig. 8. The final model consists of 10.332 vertices which build up 28.729 triangles distributed in and between 38 vertical planes.

To study the impact of uncertainties in the thickness of the soil and the geological layers on the modelling results, seven different versions of the gravimetric model were developed (Table 2). In these model versions the thicknesses of the soil layer and the disaggregated bedrock were varied in the observatory valley, at the slope and on the plateau around the Silberleite valley. The average thickness of the soil layer was changed in the valley between 1.5 and 4.5 m, at the slope between 0.05 and 0.6 m and on the plain between 0.2 and 3.0 m, whereas the average thickness of the disaggregated bedrock was varied between 9 and 21 m in the valley, between 2.5 and 5.5 m at the slope and between 4 and 16 m on the plateau. The standard deviations of the residuals between the observed and the computed free-air anomaly are listed in Table 2 to evaluate the quality of the different versions of the gravimetric modelling. Model version 3 best fits the boundary conditions (*cf.* Section 6.2), the standard deviation is the lowest one. For the version 4 it is only slightly higher. The model versions 0 and 6 show the highest standard deviations. They also do not reflect the measured thickness of the soil layer and the disaggregated bedrock. The model versions 1, 2 and 5 only marginally match the boundary conditions and lead to high standard deviations compared to the versions 3 and 4. This result verifies the quality of the static gravimetric model.

7 COMBINATION OF HYDROLOGICAL AND GRAVIMETRIC MODELLING

The output of the local process-oriented hydrological model, water storage changes in hourly time steps for the different storages in each HRU, was converted into density changes of the respective bodies of the gravimetric model using the depth information of the gravimetric model. In a zone of approximately 250 m around the observatory the HRUs of the hydrological model were transferred directly to bodies of the gravimetric 3-D model. For each HRU, the modelled water mass storage variation was applied as density change of the respective body in the layers of soil and disaggregated bedrock of the gravimetric model. Hereby, for the soil bodies the sum of the variations of the medium and large pore soil storage,

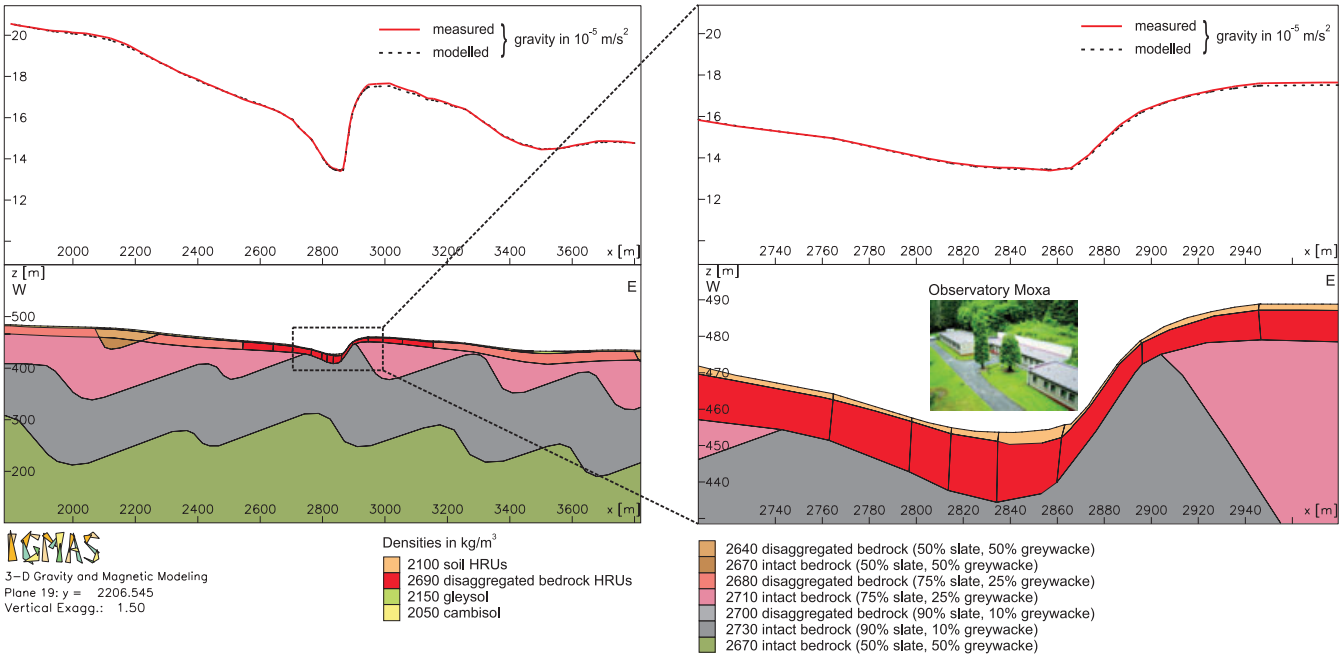

Figure 7. Left-hand panel: plane 19 (plane through observatory, *cf.* Fig. 6) of the gravimetric 3-D model including topography, soil layer, flood plain, disaggregated bedrock and intact bedrock with densities up to a distance of about 2 km around the observatory and bodies (HRUs) of the hydrological model up to a radius of 250 m around the observatory. The wavelengths and amplitudes of the folded geological layers were taken from Kasch (2006). Right-hand panel: detail of plane 19 in the immediate vicinity of the observatory. In the upper part the observed and modelled free-air anomaly is shown.

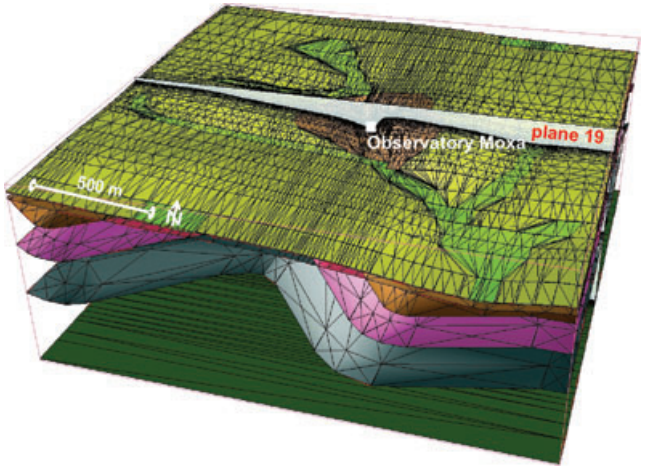

Figure 8. Triangulation of the surfaces of the gravimetric 3-D model of the observatory surroundings including topography, disaggregated and intact bedrock and soil layer. HRUs of the hydrological model are included up to a distance of 250 m from the observatory. Position of plane 19 (*cf.* Figs 6 and 7) within the model is also included. Legend is given in Fig. 7.

interception storage, snow storage and depression storage was applied, whereas for the bodies of disaggregated bedrock the variations of the ground water storage were used.

The topography was included with very high resolution as it plays an essential role regarding hydrological variations. Within the gravimetric modelling each HRU is divided into a large number of tetrahedrons with average edge lengths of about 5 m in the observatory vicinity. The gravitational effect of each of these tetrahedrons was analytically calculated. Thus, the topography is considered in detail—independently of the number and the size of the HRUs.

Previous studies (e.g. Kroner 2001; Kroner *et al.* 2004; Kroner & Jahr 2006) indicate that hydrological variations on the soil-covered roof of the observatory building might have a substantial impact on the gravity observations. However, the roof was covered in 2005 September and no short-term soil moisture variations are observed anymore and seasonal fluctuations are less than 1 per cent (Kroner 2006; Naujoks 2008; Naujoks *et al.* 2008). On the other hand, the amplitude of rain events in the gravity time-series of the superconducting gravimeter was reduced only by a few nm s^{-2}. This led to the conclusion that the origin of the main hydrological effects is not the roof, but the surroundings of the observatory. Therefore, the roof of the observatory was not implemented as a separate HRU.

In distances between 250 m and 1 km from the observatory the hydrological dynamics less affect gravity and can be assumed to be largely homogeneous regarding hydrological properties as derived from measurements. Hence, spatially averaged water storage variations of all HRUs of the hydrological model (Fig. 5) were applied to the soil layer and disaggregated bedrock bodies. By combining the local hydrological with the gravimetric model, gravity effects were computed for each gravity observation site and time step.

8 RESULTS FOR THE LOCAL NETWORK

The combined local hydrological and gravimetric modelling is validated by the observations of gravity differences on the network to ensure a realistic modelling. As in the repeated gravity difference measurements only local changes are observed (*cf.* Section 4.2) the repeated difference measurements can be directly compared to the results of the modelling. The repeated measurements with L&R gravimeters on the local network MoxaNet were carried out in a seasonal rhythm as well as at particular hydrological events like snow melt or dryness in 19 campaigns over a period of 35 months between 2004 November and 2007 September using three to

Table 2. Versions of the gravimetric model to study the impact of the thickness of the soil layer and the disaggregated bedrock on the model results.

Model version	Average thickness (m)						Derived σ of the gravimetric model ($nm\,s^{-2}$)
	Observatory valley		Steep slope		Plain		
	Soil	Disaggregated bedrock	Soil	Disaggregated bedrock	Soil	Disaggregated bedrock	
0	1.5	9	0.05	2.5	0.2	4	886
1	2.0	11	0.1	3.0	0.5	6	880
2	2.5	13	0.2	3.5	1.0	8	873
3	3.0	15	0.3	4.0	1.5	10	868
4	3.5	17	0.4	4.5	2.0	12	870
5	4.0	19	0.5	5.0	2.5	14	876
6	4.5	21	0.6	5.5	3.0	16	884

Notes: Additionally, the standard deviation σ of the residuals between the observed free-air anomaly for all gravity stations and the modelled free-air anomaly is given (*cf.* Fig. 6). The model versions 2-4 match the depth information from seismic and geoelectric measurements. Versions 3 and 4 match them best, versions 0, 1, 5 and 6 only marginally.

five selected and well-calibrated L&R gravimeters (Naujoks 2008; Naujoks *et al.* 2008). To reach the aspired accuracy, each observed gravity difference was measured 5–7 times with each gravimeter. The data were analysed by least-squares adjustment using the software package GRAVNA (Wenzel 1993). The standard deviation obtained for one adjusted gravity difference at one campaign varies from ± 9 to ± 14 nm s^{-2}, and for gravity changes between two campaigns from ± 13 to ± 20 nm s^{-2}. Hence, gravity changes obtained larger than twice the standard deviation, which ranges from ± 26 to ± 40 nm s^{-2}, are considered significant.

The observed changes in the gravity differences are displayed in Fig. 9 as red circles together with their standard deviations. The variations observed in the gravity differences correlate well with changes in local soil moisture and ground water table observations as shown by Naujoks *et al.* (2008). The gravity effect of hydrological variations is different at the various points because of the local topography and heterogeneities in the subsoil. The very local topography has in this case a big impact on the hydrological effects. The variations reflect local hydrological mass transport which opens the possibility to use them as constraints to evaluate local hydrological modelling.

From the combined local hydrogravimetric modelling temporal gravity changes were derived for all differences between the points of the MoxaNet. They are included in Fig. 9 for the model versions 1–5 described in Section 6.3. The modelled gravity differences generally show high temporal dynamics. Changes of several 10 nm s^{-2} were derived in most differences. Peaks after rain events are followed by a decay due to the water run-off. A seasonal signal can also be identified in the modelled differences reflecting a generally dry situation in summer and a wetter situation in winter months. Additionally, in Fig. 9 the standard deviation of the observations is given. Taking into account twice the standard deviation most of the modelling results are within this limit.

Between the results of the modelling for the different versions of the combined hydrogravimetric model significant deviations of up to 80 nm s^{-2} occur. Model version 1 shows the smallest variations, whereas the variations caused by model version 5 are by a factor of two larger. The variations of the model versions 3–4 are in between. A comparison of the standard deviations between measured and modelled gravity changes is given in Table 3. For the calculation, the gravity changes in all differences between all campaigns (except campaigns 1–4, 13 and 14) were considered. The campaigns 1–4 were excluded from the calculations as the network configuration was still tested during theses campaigns and different instruments were checked (Naujoks *et al.* 2008). During campaigns 13 and 14 strong wind and an earthquake disturbed the measurements. Therefore, the results of these campaigns are less reliable.

From the standard deviations given in Table 3 it can be deduced that model versions 3 and 4 of the combined hydrological and gravimetric model correspond to the observations best. This shows clearly that the results of the hydrological modelling most exactly match the gravity observations when the gravimetric model fulfils the boundary conditions best of all. For model version 2, and, in particular 1 and 5, the standard deviation is higher. Model version 1 and 2 underestimates the observed changes, model version 5 overestimates them. Because these model versions only marginally reflect the boundary conditions (Section 6.2) and their standard deviation of the residuals between measured and modelled free-air anomaly in the gravimetric model is high (Table 2), they are not realistic and are excluded from further considerations. Thus, the important conclusion can be drawn that the most plausible geometries give the best information on local hydrology. The standard deviations considering only the differences within the valley, to the point on the hill and to the point on the roof are also given in Table 3. The standard deviations are minimum for the differences in the valley and maximum for the differences to the observatory roof.

The general behaviour of the observed and modelled gravity differences is discussed exemplarily for the changes in the differences between the two successive campaigns 5 and 6 which represent typical different hydrological situations: campaign 5 was during snow melt 2005, campaign 6 during dry summer 2005. The general discussion and statements can be transferred similarly to the other campaigns.

8.1 Differences to the point on the hill

In the gravity differences between the points within the Silberleite valley and the point ET on the hill the largest changes of 171 nm s^{-2} were observed during the repeated campaigns (Figs 9a–d). The changes are maximum for the differences containing the points AG and SG, both situated in the observatory building at the foot of the slope, and decrease for the differences from the points in the valley with increasing distance to the slope. For the difference from the points SG and AG to the point ET on the slope they reach 106 and 136 nm s^{-2}, respectively. In the difference MB–ET a maximum change of 35 nm s^{-2} was observed, and for the difference WE–ET, 18 nm s^{-2}. In the difference DA–ET (Fig. 9e) also strong changes were observed, they amount up to 46 nm s^{-2} between campaigns 5 and 6 and up to 153 nm s^{-2} among all campaigns.

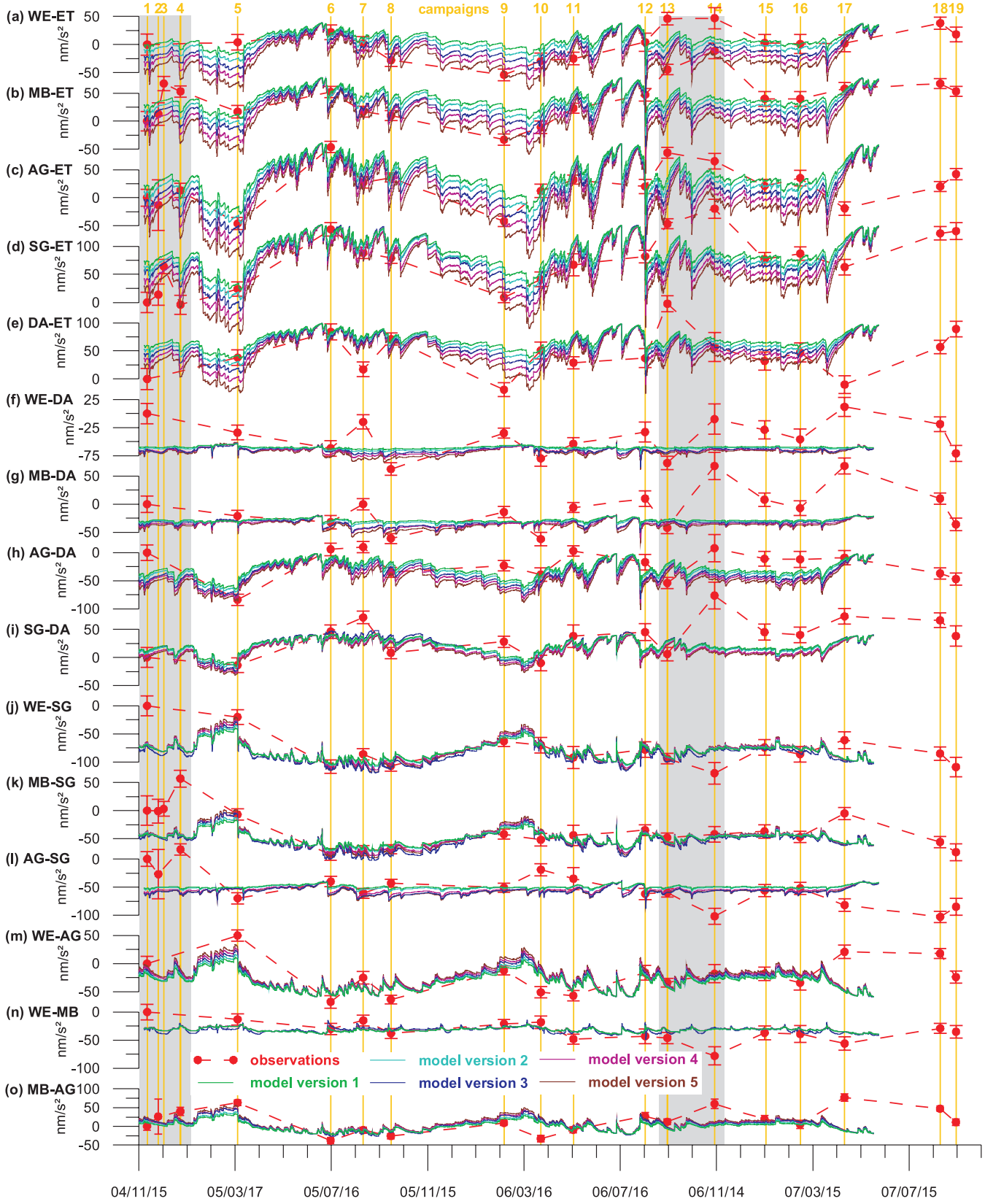

Figure 9. Temporal changes in the observed gravity differences (red circles) with standard deviation and modelled hydrologically induced variations in the differences between several points around the observatory (*cf.* Fig. 2) for five different model versions (*cf.* Table 2). The grey boxes mark measurement campaigns with less reliable data.

Table 3. Standard deviations σ between observation and modelling calculated for the gravity differences in the local network for the different model versions.

Considered differences	σ (nm s^{-2}) for the model versions				
	1	2	3	4	5
All	25.8	25.3	25.0	25.1	25.4
In the valley	24.7	24.6	24.5	24.6	24.7
To point ET	28.2	26.3	25.8	26.1	26.8
To point DA	31.2	31.1	31.0	31.0	31.2

In correspondence to the observations, in the modelled gravity differences the largest changes occur also in the differences to the point ET. Seasonal variations are prominent. During wet conditions in winter, the modelled gravity differences are several 10 nm s^{-2} smaller than in the dry summer months. The changes are maximum in the differences SG–ET and AG–ET, and by a factor two smaller in the differences MB–ET and WE–ET. Between the campaigns 5 and 6 a clear increase reaching 160 nm s^{-2} was found in the modelled gravity differences corresponding to the observed variations. These observed and modelled changes can be explained by hydrological processes acting between and in the area around the points. Thus, hydrological processes in the hill slope have a crucial impact on the modelled as well as the observed gravity changes in the differences. These results corroborate that hydrological processes in the steep slope have a crucial impact on gravity.

8.2 Differences to the point on the observatory roof

The observed and modelled differences from points in the observatory valley to point DA on the roof, given in Figs 9(f)–(i), also show seasonal variations and similar characteristics like the differences from points in the observatory valley to point ET. In general, the variations are by a factor of two to three smaller compared to those to the point ET.

For the difference SG–DA the observed changes reach 60 nm s^{-2} between the campaigns 5 and 6, and for the difference AG–DA 90 nm s^{-2}. For the differences from the points MB and WE to the observatory roof they are generally smaller: they amount up to 11 nm s^{-2} for the difference MB–DA, and 28 nm s^{-2} for the difference WE–DA. These results support the consideration that the slope between the points in the valley and the point ET on the hill plays a crucial role in the changes of the gravity differences.

The modelling results do, however, not always behave uniformly and do not always match the observations: for the differences from the points outside the observatory building in the middle of the valley (WE–DA and MB–DA) only small variations of less than 40 nm s^{-2} were derived from the modelling, whereas the observations show changes up to 95 nm s^{-2}. In contrast, the modelled differences from the points in the building at the steep slope (AG–DA and SG–DA) show larger variations up to 100 nm s^{-2} widely corresponding to the observations. These results indicate that either the points WE, MB and DA are situated in a similar hydrological regime which is not confirmed by the observations, or the hydrological dynamics in the observatory valley are not fully explained by the hydrological model. The latter is supported by slightly higher standard deviations between observation and modelling (Table 3) for these differences. Here, further hydrological research may commence evaluating also the feasibility of setting up a physically based hydrological model for this defined area.

8.3 Differences between points in the valley

The changes in the differences between the points in the valley are given in Figs 9(j)–(o). In the differences AG–SG and WE–MB only very small changes were observed. From the combined modelling also small changes of less than 20 nm s^{-2} were derived in these differences generally corresponding to the observations. Seasonal variations are nearly completely cancelled out in these differences.

In contrast, in the differences WE–SG, MB–SG, WE–AG and MB–AG – with always one point situated in the observatory building close to the slope and one outside – larger changes occur. From the modelling changes of about 80 nm s^{-2} maximum were derived which widely correspond to the observations. In these differences the seasonal signal is visible. During wet conditions in winter months the observed and modelled gravity differences are approximately 60 nm s^{-2} larger than in the dry summer months.

These different changes between the various points might be caused by the particular location of the gravity stations: the points AG and SG are located in the observatory building, both points WE and MB outside, each pair of points close together in an almost identical hydrological regime and in a similar distance to the steep slope. This indicates that the points within the building are differently affected by local hydrology than the points outside the building. However, the measured and modelled changes between the points in the valley are still too small to be significant, but they are consistent with one another and trends can be identified. These results confirm that the hydrological situation around the observation points is correctly implemented in the hydrological model. This is also confirmed by the small standard deviation of 24.5 nm s^{-2} between observations and modelling results for model version 3 for the differences in the valley (Table 3) which is also in the order of the observed standard deviations.

However, the observed and modelled gravity changes partially significantly differ from each other, for example in the difference MB–AG (Fig. 9o) between the campaigns 9 and 10. This may be explained by the fact that the observation sites AG and SG are situated inside the observatory building where the soil is sealed. Hence, no water can infiltrate in the subsoil in this area. Below the observatory building, however, water flow is observed during strong rain events or snow melt (Kroner *et al.* 2007). Thus, a special short-term impact on the local hydrological processes should be expected which may be even better considered in the hydrological modelling in future.

8.4 General findings

The modelled gravity variations reflect the observed changes very well within the standard deviations. They are in the right order of magnitude and follow the same direction as the observations. Thus, the modelled hydrological changes generally well reflect the hydrological changes in the surroundings of the gravity observation sites for most campaigns and in most differences. In particular, the modelling reproduces the variations in the differences between points within the Silberleite valley very well; the standard deviation between observation and modelling is 24.5 nm s^{-2}. The changes in the differences between points in the observatory valley and point ET could also be satisfactorily explained.

The modelled variations in the gravity differences from points in the valley to the point on the hill are by a factor of about two to three larger than the variations in the differences to the observatory roof or in the valley. The stronger the changes in the topography between the observation points, the larger are the gravity changes.

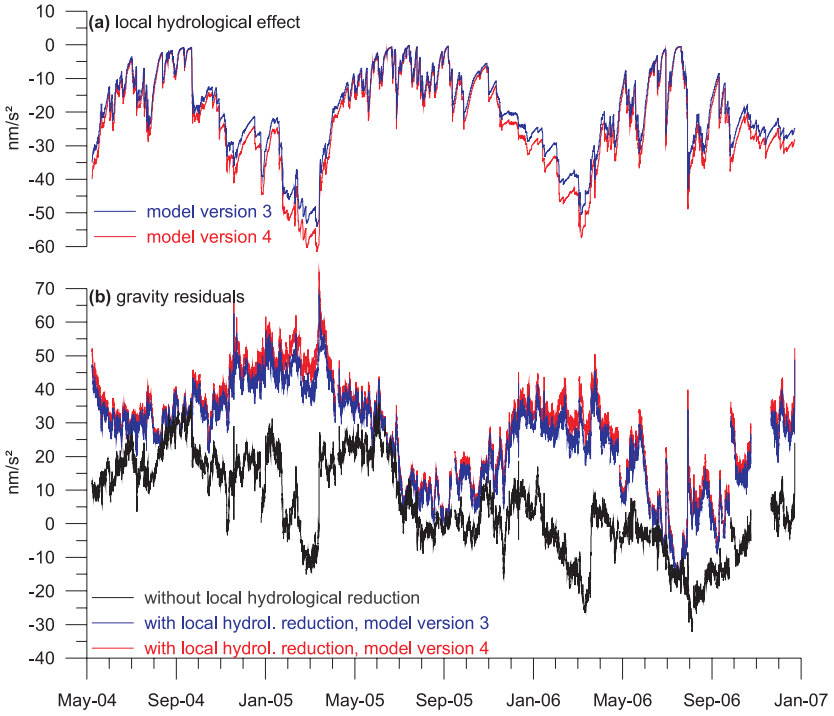

Figure 10. (a) Local hydrological effect derived from the local hydrological and gravimetric 3-D model for the location of the superconducting gravimeter at Moxa observatory. (b) Gravity residuals of the superconducting gravimeter without (black) and with local hydrological reduction.

This supports the results of the observations that, in particular, hydrological processes in the steep slope east of the observatory between the points in the valley and point ET on the hill have an essential impact on the gravity differences. They are mainly induced by the topographic setting but also by heterogeneities of the subsoil. Because the differences from the observatory roof to the points in the valley as well as to the point on the hill show large variations, these hydrological processes must be active above and below the level of the observatory roof.

9 RESULTS FOR THE LOCATION OF THE SUPERCONDUCTING GRAVIMETER

Further information can be gained by comparing the gravity residuals obtained from the superconducting gravimeter observations with the modelled local hydrological effect for the location of this instrument.

9.1 Local considerations

As for the gravity stations of the MoxaNet (Section 8), the impact of different thicknesses of the soil layers and the disaggregated bedrock on the hydrological effect for the location of the superconducting gravimeter was studied. The results for those model versions that fit the boundary conditions and the observations in the MoxaNet are given in Fig. 10(a) for the period from 2004 May to 2006 December. A seasonal signal can be identified in the modelled hydrological effect. For model version 3, a maximum amplitude of -54 nm s^{-2} was derived for the entire local hydrological effect. For model version 4 this amplitude is -61 nm s^{-2}. The maximum amplitudes in winter are mainly caused by high water content in the soil and the disaggregated bedrock as well as snow cover. The effect has a negative sign because most of the surroundings of the observatory are above the gravimeter level (*cf.* Section 4.1).

The gravity residuals of the superconducting gravimeter without hydrological reduction are shown in Fig. 10(b) in black. A clear seasonal signal is not visible in the data but effects due to snow can be identified. Each year in winter snow accumulation and a high soil water content cause the gravity to decrease, at snow melt in 2005 and 2006 mid-March gravity increases rapidly. A thick snow cover in 2005 winter with a maximum snow depth of approximately 50 cm caused a gravity decrease in 2005 February/March of about 30 nm s^{-2}; at snow melt 2005 mid-March gravity increased rapidly by the same amount within one day.

From these data the local hydrological effect – computed with the model versions 3 and 4 – was subtracted. In the resulting gravity residuals (Fig. 10b) a seasonal variation emerges with a maximum peak-to-peak amplitude of approximately 66 nm s^{-2} for model version 3, and 72 nm s^{-2} for model version 4, respectively. Thus, the maximum hydrological effect between model version 3 and 4 varies by ± 3 nm s^{-2} showing the uncertainty due to the structure of the combined model. However, a possible additional uncertainty due to the hydrological model may arise. In the original gravity data this seasonal effect is superimposed by the effect of local hydrology. Particularly during the wet winter months this local masking effect is strongly developed. This phenomenon is prominent at Moxa observatory because most of the local topography is above gravimeter level and most of the large-scale one below.

For a few short-term events the local hydrological variations cannot be sufficiently eliminated from the gravity data yet. For instance, the strong gravity changes at the snow melt in the years 2005 and 2006 cannot be fully explained by the current local hydrological reduction (Fig. 10). Particularly the strong gravity gradient 2005 and 2006 mid-March, but also some strong gradients after rain events

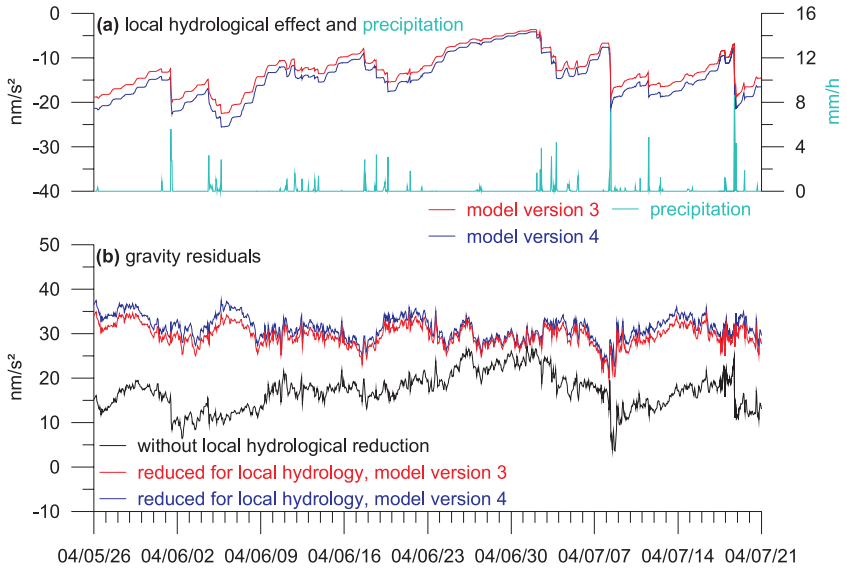

Figure 11. (a) Modelled local hydrological effect and precipitation data for comparison for the period from 2004 May 26 to 2004 July 20; (b) gravity residuals without (black) and with local hydrological reduction.

are reproduced time-delayed by the hydrological model, resulting in strong but short-term peaks (up to 15 nm s^{-2}) in the respective local hydrology reduced gravity data (Fig. 10b).

In Fig. 11(a) detail of the time-series over a summer period of 2 months from 2004 May 26 to 2004 July 20 is given. The modelled local hydrological effect is compared to precipitation data (Fig. 11a) and to the gravity residuals (Fig. 11b). At rain events with successive high water table and soil moisture water mass is first stored above the gravimeter level, leading to a fast gravity decrease. While the water is moving downwards below the gravimeter level, gravity successively increases. About a dozen rain events occurred during this period. They give clear signals in the modelled local hydrological effect of up to -23 nm s^{-2} for model version 3, and -26 nm s^{-2} for version 4, respectively. Single rain events caused a local hydrological effect of up to -12 nm s^{-2} for model version 3, and -14 nm s^{-2} for version 4. The rain events also can be clearly identified as a strong gravity drop of some nanometres per square seconds in the gravity residuals before the local hydrological reduction, for example, on 2004 June 1 or on 2004 July 18. After subtraction of the modelled local hydrological effect from the gravity residuals, the effect of the rain events is largely reduced for most events. In general, 80–90 per cent of the variations caused by short-term events are removable in this first step of hydrological modelling.

9.2 Large-scale considerations

Besides local also large-scale storage variations can be studied. The superconducting gravimeter data are recorded each second. After filtering to minute samples and processing, the SG data are decimated to hourly values (Kroner 2001). In contrast, GRACE gravity field solutions and data from global hydrological models are available as monthly values. To bridge this gap in temporal resolution, monthly arithmetic means were calculated from the continuous gravimeter data without and with local hydrological reduction with model version 3 and 4 (Fig. 12a).

A comparison between the terrestrial gravity data from Moxa station, GRACE satellite-derived gravity field variations for a Gauss filtering with $\ell_{\mathrm{fl}} = 10$ and $\ell_{\mathrm{fl}} = 13$, respectively (Neumeyer *et al.* 2006, 2008; Weise *et al.* 2009), and gravity changes based on the Water-GAP Global Hydrology Model (WGHM) (Döll *et al.* 2003) is given in Fig. 12(b). The total non-local seasonal hydrological effect amounts to 35–40 nm s^{-2} which is a well-resolvable signal in terrestrial gravity observations in mid-Europe on condition that – if needed – a local hydrological influence is appropriately removed first. In the Moxa gravity residuals without local hydrological reduction this seasonal signal is not reflected. Thus, only the appropriate reduction of the local hydrological influence reveals variations related to changes in continental water storage on a larger scale. A good agreement exists between the terrestrial data and the GRACE solutions. The WGHM, applied to calculate gravity contributions caused by continental water storage changes, represents the most important continental water storage compartments (snow, soil moisture, ground water and surface water in rivers, lakes and wetlands) at a spatial resolution of 0.5° with global coverage in monthly time steps (Güntner *et al.* 2007a,b). Gravity changes from the WGHM and observed variations generally coincide as well. Thus, the seasonal variation, which becomes visible in the Moxa terrestrial gravity data after removing the local hydrological effect can be assumed to be mainly due to mass changes in regional and global continental water storage. Apart from the correspondence in principle between the various time-series, minor deviations with respect to amplitudes and phases occur. With regard to these deviations further research may commence with the goal to derive constraints from terrestrial and satellite gravity observations for an improvement of regional and global hydrological models.

In general both, terrestrial and satellite data contain valuable information on mass transfer, especially on hydrological mass phenomena. Thus, they can be deployed for the assessment and evaluation of regional and global hydrological models.

10 DISCUSSION AND CONCLUSIONS

Temporal gravity field observations are affected by hydrological mass variations. For the first time it was investigated to what extent hydrological signals in terrestrial gravity data can provide constraints for hydrological process research and whether they may

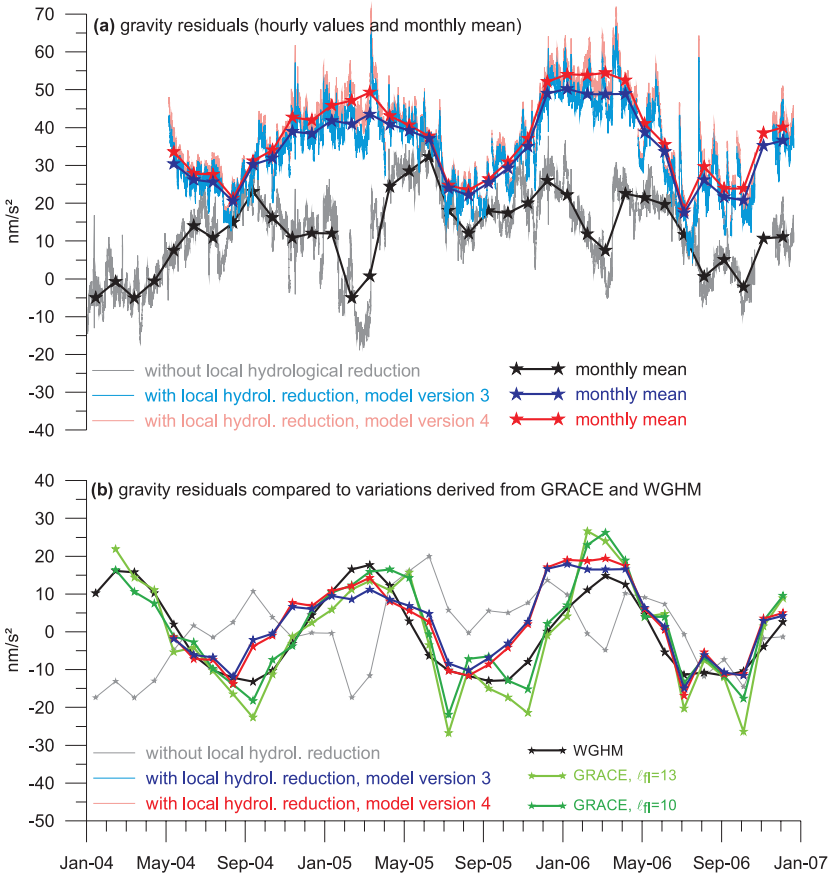

Figure 12. (a) Gravity variations of the superconducting gravimeter at Moxa without and with local hydrological reduction (model version 3 and 4, *cf.* Table 2) in hourly values and monthly means; (b) Comparison of the monthly means of the gravity residuals from the superconducting gravimeter at Moxa with monthly GRACE solutions using different filtering and gravity variations derived from changes in continental water storage computed with the WGHM for Moxa. The deformation part due to global hydrology, which is not seen by the satellite, has been added to the GRACE-based temporal gravity changes. For technical details regarding GRACE and WGHM data processing *cf.* Neumeyer *et al.* (2006, 2008), and Weise *et al.* (2009) where the data are taken from.

serve for evaluating hydrological models on a local scale. Vice versa hydrological variations need to be eliminated from the gravimeter data to detect small geodynamic signals. Thus, a reduction basing on a local hydrological model was developed. These were the two central objectives of this study.

At the Geodynamic Observatory Moxa, hydrologically induced gravity variations are observed with a superconducting gravimeter and with spatially distributed measurements with portable relative gravimeters. The observed hydrological effects result from the temporally and spatially variable water contents in the various compartments of the hydrological system. For a more detailed assessment, spatial and temporal density changes of the soil and disaggregated bedrock were simulated numerically with a gravimetric 3-D model of the observatory surroundings by integrating spatially and temporally distributed hydrological inputs obtained from a process-oriented hydrological model of the surrounding catchment.

From the comparison of the modelled gravity effects at the different observation points obtained from the combined hydrogravimetric modelling, the observed gravity differences from the repeated campaigns, and the superconducting gravimeter residuals, the following conclusions can be drawn.

(i) Hydrologically caused gravity variations of tens of nanometres per square second, modelled for the locations of the MoxaNet correspond well with the results of the repeated and spatially distributed high-precision gravity difference measurements from short-term to seasonal scales.

(ii) For an adequate description of the contribution of hydrological effects in the superconducting gravimeter data the local surroundings are of high importance as both, observation and modelling clearly show that strong hydrological variations in the steep slope east of the observatory have a major impact on gravity.

(iii) The hydrological variations are mainly induced by the topographic setting with flow processes in the disaggregated bedrock but also by heterogeneities of the subsoil.

(iv) With the integrated methodology a successful reduction of the local hydrological effect in the data of the superconducting gravimeter was achieved including short-term and seasonal variations with an uncertainty in the seasonal amplitude of ± 3 nm s^{-2} due to the structure of the combined model.

(v) The residuals after this reduction show a clear seasonal amplitude of 35–40 nm s^{-2} which was masked in the data by the local hydrology. This signal corresponds well to the seasonal variations of GRACE data and global hydrological models, indicating a regional/global origin.

(vi) The combination of a local hydrological model with a gravimetric 3-D model provides a better understanding of hydrologically induced gravity variations.

Despite the promising results some open research questions remain which have to be tackled in the future.

(i) The large influence of the hydrological processes on the steep eastern slope on the gravimeter measurements should be considered by more detailed investigations, by more hydrological measurements which enable an even finer distributed hydrological modelling in high temporal resolution.

(ii) The impact of hydrological effects from underneath the observatory building needs to be studied in more detail as it is very likely causing some of the deviations between observations and modelling results in the gravity differences between points in the valley.

(iii) The comparison of simulated gravity effects of snow melt and heavy rain events with the observations of the superconducting gravimeter show a systematic delay of a few hours. This information along with hydrological field measurements can be used to validate and improve the infiltration routine and the lateral subsurface routing process representation in the hydrological model which are responsible for this delay. Additionally, the modelled gravity effect over- and underestimates the observed gravity values in some specific periods. The detailed analysis of the spatial and temporal patterns of such deviations will provide important information for a better representation of small-scale hydrological process dynamics in the hydrological model.

As a general conclusion it can be stated that a joint evaluation of process-based hydrological modelling and gravity observations in combination with gravimetric 3-D modelling provides important information on a local scale. This study shows that the accuracy of such evaluation depends strongly on the quality of the gravity data, the spatial and temporal resolution of the local model, the process representation of the hydrological model and how accurate the output of the hydrological model can be translated into gravity changes. As a welcome effect this study provided hints for some modifications of the involved modelling components which will help in a further improvement of the process representation in the hydrological model and the local hydrological reduction for the superconducting gravimeter record. Finally, it can be concluded that such a kind of investigation is worth to be done for each station where high-precision gravity measurements are being performed and local hydrological variations are to be expected, to improve the signal-to-noise ratio and conversely, to possibly provide valuable information on hydrological processes and constraints to hydrological modelling.

ACKNOWLEDGMENTS

Without the contribution of a number of persons, the extensive fieldwork would not have been possible. We thank Raphael Dlugosch, Manfred Fink, Holger Hartmann, Katrin Heinzig, Anne Hegewald, Gerhard Jentzsch, Norbert Kasch, Martin Rasmussen, Romy Schmidt, Stefanie Zeumann and Albrecht Ziegert from the Friedrich-Schiller-University Jena for their help. We are indebted to the Institute of Geodesy and Geoinformation Technology of the Technical University Berlin and the Leibniz Institute for Applied Geosciences for lending us their instruments. We gratefully acknowledge Hans-Jürgen Götze and Sabine Schmidt from the Christian-Albrechts-University Kiel for valuable discussions on gravimetric reductions and gravimetric modelling. We are especially indebted to Sabine Schmidt for providing a special IGMAS version which was essential for the time-dependent calculations. The work of Wernfrid Kühnel and Matthias Meininger from Moxa observatory in establishing and maintaining the hydrological observation network is gratefully acknowledged and the discussion with Roel Dijksma from Wageningen University shed some more light on the local hydrology at Moxa. Finally, we thank the reviewers for constructive comments and valuable suggestions which improved the paper considerably. This research was supported by the German Research Foundation (DFG) by grants KR 1906/6-1-2-3.

REFERENCES

Abe, M. *et al.*, 2006. Hydrological effects on the superconducting gravimeter observation in Bandung, *J. Geodyn.,* **41**(1–3), 288–295, doi:10.1016/j.jog.2005.08.030.

Abe, M., Kroner, C., Neumeyer, J. & Chen, X.D., 2010. Assessment of atmospheric reductions for terrestrial gravity observations, *Bulletin d'Information des Marées Terrestres,* **146,** 11 817–11 838.

Amalvict, A., Hinderer, J., Mäkinen, J., Rosat, S. & Rogister, Y., 2004. Long-term and seasonal gravity changes at the Strasbourg station and their relation to crustal deformation and hydrology, *J. Geodyn.,* **38**(3–5), 343–353, doi:10.1016/j.jog.2004.07.010.

Bonatz, M., 1967. Der Gravitationseinfluß der Bodenfeuchte, *Zeitschrift für Vermessungswesen,* **92,** 135–139.

Bower, D. & Courtier, N., 1998. Precipitation effects on gravity measurements at the Canadian absolute gravity site, *Phys. Earth planet. Inter.,* **106**(3–4), 353–369, doi:10.1016/S0031-9201(97)00101-5.

Boy, J.-P. & Hinderer, J., 2006. Study of the seasonal gravity signal in superconducting gravimeter data, *J. Geodyn.,* **41**(1–3), 227–233, doi:10.1016/j.jog.2005.08.035.

Creutzfeldt, B., Güntner, A., Klügel, T. & Wziontek, H., 2008. Simulating the influence of water storage changes on the superconducting gravimeter of the Geodetic Observatory Wettzell, Germany, *Geophysics,* **73**(6), WA95–WA104, doi:10.1190/1.2992508.

Crossley, D.J., Xu, S. & van Dam, T., 1998. Comprehensive analysis of 2 years of SG data from Table Mountain, Colorado, in *Proceedings of the 13th International Symposium on Earth Tides,* pp. 659–668, Observatoire Royal de Belgique, Brussels, Schweizerbart'sche Verlagsbuchhandlung.

Crossley, D.J. *et al.*, 1999. Network of superconducting gravimeters benefits a number of disciplines, *EOS, Trans. Am. geophys. Un.,* **80**(11), 121–126, doi:10.1029/99EO00079.

Döll, P., Kaspar, F. & Lehner, B., 2003. A global hydrological model for deriving water availability indicators: model tuning and validation, *J. Hydrol.,* **270,** 105–134, doi:10.1016/S0022-1694(02)00283-4.

Elstner, C. & Kautzleben, H., 1982. Results of annual gravity measurements along a W–E profile inside the GDR for the period 1970–1980, in *Proceedings of the General Meeting of the IAG,* Tokyo, pp. 341–348.

Götze, H.-J., 1976. Ein numerisches Verfahren zur Berechnung der gravimetrischen Feldgrößen für dreidimensionale Modellkörper, *PhD thesis*, Institute of Geophysics, TU Clausthal.

Götze, H.-J., 1984. Über den Einsatz interaktiver Computergraphik im Rahmen 3-dimensionaler Interpretationstechniken in der Gravimetrie und der Magnetik, *Habilitation thesis*, Institute of Geophysics, TU Clausthal.

Götze, H.-J. & Lahmeyer, B., 1988. Application of three-dimensional interactive modelling in gravity and magnetics, *Geophysics,* **53**(8), 1096–1108, doi:10.1190/1.1442546.

Güntner, A., Schmidt, R. & Döll, P., 2007a. Supporting large-scale hydrogeological monitoring and modelling by time-variable gravity data, *Hydrogeol. J.,* **15**(1), 167–170, doi:10.1007/s10040-006-0089-1.

Güntner, A., Stuck, J., Werth, S., Döll, P., Verzano, K. & Merz, B., 2007b. A global analysis of temporal and spatial variations in continental water storage, *Water Resour. Res.,* **43**(5), W05416, doi:10.1029/2006WR005247.

Harnisch, G. & Harnisch, M., 2006. Hydrological influences in long gravimetric data series, *J. Geodyn.,* **41**(1–3), 276–287, doi:10.1016/j.jog.2005.08.018.

Harnisch, M. & Harnisch, G., 1999. Hydrological influences in the registrations of superconducting gravimeters, *Bulletin d'Information des Marées Terrestres,* **131,** 10 161–10 170.

Hasan, S., Troch, P., Boll, J. & Kroner, C., 2006. Modeling of the hydrological effect on local gravity at Moxa, Germany, *J. Hydrometeor.,* **7**(3), 346–354, doi:10.1175/JHM488.1.

Hasan, S., Troch, P., Bogaart, P. & Kroner, C., 2008. Evaluating catchment-scale hydrological modeling by means of terrestrial gravity observations, *Water Resour. Res.,* **W08416,** doi:10.1029/2007WR006321.

Hokkanen, T., Korhonen, K., Virtanen, H. & Laine, E.L., 2007. Effects of the fracture water of bedrock on superconducting gravimeter data, *Near Surf.Geophys.,* **5**(2), 133–140.

Imanishi, Y., 2000. Present status of SG T011 at Matsushiro, Japan, *Cahiers du Centre Européen de Géodynamique et de Séismologie,* **17,** 97–102.

Imanishi, Y., Kokubo, K. & Tatehata, H., 2006. Effect of underground water on gravity observation at Matsushiro, Japan, *J. Geodyn.,* **41,** 221–226, doi:10.1016/j.jog.2005.08.031.

Jacob, T., Chery, J., Bayer, R., Moigne, N.L., Boy, J.-P., Vernant, P. & Boudin, F., 2009. Time-lapse surface to depth gravity measurements on a karst system reveal the dominant role of the epikarst as a water storage entity, *Geophys. J. Int.,* **177**(2), 347–360, doi:10.1111/j.1365-246X.2009.04118.x.

Jahr, T., Jentzsch, G. & Kroner, C., 2001. The Geodynamic Observatory Moxa / Germany: instrumentation and purposes, *J. Geod. Soc. Jpn.,* **47**(1), 34–39.

Kasch, N., 2006. Geologische Neukartierung der Umgebung des Geodynamischen Observatoriums Moxa, *Diploma thesis,* Institute of Geosciences, Friedrich-Schiller-University Jena.

Krause, P., 2001. Das hydrologische Modellsystem J2000: Beschreibung und Anwendung in großen Flußeinzugsgebieten, in *Schriften des Forschungszentrums Jülich: Reihe Umwelt/Environment,* Vol. 29, Forschungszentrum Jülich.

Krause, P., Bende-Michl, U., Bäse, F., Fink, M., Flügel, W. & Pfennig, B., 2006. Multiscale investigations in a mesoscale catchment—hydrological modelling in the Gera catchment, *Adv. Geosci.,* **9,** 53–61.

Krause, P., Naujoks, M., Fink, M. & Kroner, C., 2009. The impact of soil moisture changes on gravity residuals obtained with a superconducting gravimeter, *J. Hydrol.,* **373**(1–2), 151–163, doi:10.1016/j.jhydrol.2009.04.019.

Kroner, C., 2001. Hydrological effects on gravity data of the Geodynamic Observatory Moxa, *J. Geod. Soc. Japan,* **47**(1), 353–358.

Kroner, C., 2006. Hydrological signals in the SG records at Moxa—a follow up, *Bulletin d'Information des Marées Terrestres,* **142,** 11 353–11 358.

Kroner, C. & Jahr, T., 2006. Hydrological experiments around the superconducting gravimeter at Moxa Observatory, *J. Geodyn.,* **41**(1–3), 268–275, doi:10.1016/j.jog.2005.08.012.

Kroner, C., Jahr, T. & Jentzsch, G., 2004. Results of 44 months of observations with a superconducting gravimeter at Moxa/Germany, *J. Geodyn.,* **38**(3–5), 263–280, doi:10.1016/j.jog.2004.07.012.

Kroner, C., Jahr, T., Naujoks, M. & Weise, A., 2007. Hydrological signals in gravity—foe or friend? in *Dynamic Planet—Monitoring and Understanding a Dynamic Planet with Geodetic and Oceanographic Tools,* IAG Symp. Ser., Vol. 130, pp. 504–510, Springer, Berlin, doi:10.1007/978-3-540-49350-1.

Kroner, C., Thomas, M., Dobslaw, H., Abe, M. & Weise, A., 2009. Seasonal effects of non-tidal oceanic mass shifts in observations with superconducting gravimeters, *J. Geodyn.,* **48**(3–5), 354–359, doi:10.1016/j.jog.2009.09.009.

Lambert, A. & Beaumont, C., 1977. Nano variations in gravity due to seasonal groundwater movements; implications for the gravitational detection of tectonic movements, *J. Geophys. res.,* **82**(2), 297–306, doi:10.1029/JB082i002p00297.

Llubes, M., Florsch, N., Hinderer, J., Longuevergne, L. & Amalvict, M., 2004. Local hydrology, the Global Geodynamics Project and CHAMP/GRACE perspective: some case studies, *J. Geodyn.,* **38**(3–5), 355–374, doi:10.1016/j.jog.2004.07.015.

Longuevergne, L., Boy, J.P., Florsch, N., Viville, D., Ferhat, G., Ulrich, P., Luck, B. & Hinderer, J., 2009. Local and global hydrological contributions to gravity variations observed in Strasbourg, *J. Geodyn.,* doi:10.1016/j.jog.2009.09.008.

Mäkinen, J. & Tattari, S., 1988. Soil moisture and groundwater: two sources of gravity variations, *Bulletin d'Information, Bureau Gravimetrique International,* **63,** 103–110.

Mäkinen, J. & Tattari, S., 1991. The influence of variation in subsurface water storage on observed gravity, in *Proceedings of 11th International Symposium Earth Tides, 1989,* pp. 457–471, Schweizerbart'sche Verlagsbuchhandlung, Stuttgart.

Merlet, S., Kopaev, A., Diament, M., Geneves, G., Landragin, A. & Pereira Dos Santos, F., 2008. Micro-gravity investigations for the LNE watt balance project, *Metrologia,* **45,** 265–274, doi:10.1088/0026-1394/45/3/002.

Meurers, B., Van Camp, M. & Petermans, T., 2007. Correcting superconducting gravity time-series using rainfall modelling at the Vienna and Membach station and application to Earth tide analysis, *J. Geod.,* **81**(11), 703–712, doi:10.1007/s00190-007-0137-1.

Monteith, J.L., 1975. *Vegetation and Atmosphere,* Vol. 1, Principles, Academic Press, London.

Nash, J.E. & Sutcliffe, J.V., 1970. River flow forecasting through conceptual models part I: a discussion of principles, *J. Hydrol.,* **10**(3), 282–290, doi:10.1016/0022-1694(70)90255-6.

Naujoks, M., 2008. Hydrological information in gravity: observation and modelling, *PhD thesis*, Institute of Geosciences, Friedrich-Schiller-University Jena, URL: http://www.db-thueringen.de/servlets/DerivateServlet/Derivate-16661/Naujoks/Dissertation.pdf.

Naujoks, M., Weise, A., Kroner, C. & Jahr, T., 2008. Detection of small hydrological variations in gravity by repeated observations with relative gravimeters, *J. Geod.,* **82,** 543–553, doi:10.1007/s00190-007-0202-9.

Neumeyer, J. *et al.*, 2006. Combination of temporal gravity variations resulting from superconducting gravimeter (SG) recordings, GRACE satellite observations and global hydrology models, *J. Geod.,* **79**(10–11), 573–585, doi:10.1007/s00190-005-0014-8.

Neumeyer, J., Schmidt, T. & Stöber, C., 2007. Improved determination of the atmospheric attraction with 3D air pressure density data and its reduction on ground gravity measurements, in *Dynamic Planet: Monitoring and Understanding a Dynamic Planet with Geodetic and Oceanographic Tools,* IAG Symp. Ser., Vol. 130, Springer, Berlin, doi:10.1007/978-3-540-49350-1_79.

Neumeyer, J., Barthelmes, F., Kroner, C., Petrovic, S., Schmidt, R., Virtanen, H. & Wilmes, H., 2008. Analysis of gravity field variations derived from superconducting gravimeter recordings, GRACE satellite and hydrological models at selected European sites, *Earth, Planets Space,* **60**(5), 1–14.

Peter, G., Klopping, F. & Berstis, K., 1995. Observing and modeling gravity changes caused by soil moisture and groundwater table variations with superconducting gravimeters in Richmond, Florida, U.S.A., *Cahiers du Centre Européen de Géodynamique et de Séismologie,* **11,** 147–159.

Rosat, S., Hinderer, J., Crossley, D. & Boy, J., 2004. Performance of superconducting gravimeters from long-period seismology to tides, *J. Geodyn.,* **38**(3–5), 461–476, doi:10.1016/j.jog.2004.07.005.

Sato, T., Boy, J.-P., Tamura, Y., Matsumoto, K., Asari, K., Plag, H.-P. & Francis, O., 2006. Gravity tide and seasonal gravity variation at Ny-Ålesund, Svalbard in Arctic, *J. Geodyn.,* **41**(1–3), 234–241, doi:10.1016/j.jog.2005.08.016.

Schmidt, S., 1996. 3D Modelling of geoid and gravity using GIS-functions, *Österreichische Beiträge zur Meteorologie und Geophysik, Wien,* **14,** 137–144.

Schmidt, S., 2000. IGMAS — Interactive Gravity and Magnetic Application System, Online Manual, http://www.gravity.uni-kiel.de/igmas/, last access 2009 May12.

Scholten, T. *et al.*, 2004. Bodenkundliche Karte 1:10 000 für das Einzugsgebiet der Silberleite am Geodynamischen Observatorium Moxa, soilmap, unpublished.

Van Camp, M., Vanclooster, M., Crommen, O., Petermans, T., Verbeeck, K., Meurers, B., van Dam, T. & Dassargues, A., 2006. Hydrogeological investigations at the Membach station, Belgium, and application to correct long periodic gravity variations, *J. geophys. Res.,* **111,** B10403, doi:10.1029/2006JB004405.

Virtanen, H., 2000. On the observed hydrological environmental effects on gravity at the Metsähovi station, Finland, *Cahiers du Centre Européen de Géodynamique et de Séismologie,* **17,** 169–176.

Virtanen, H., Tervo, M. & Bilker-Koivula, M., 2006. Comparison of superconducting gravimeter observations with hydrological models of various spatial extents, *Bulletin d'Information des Marées Terrestres,* **142,** 11361–11368.

Weise, A., Kroner, C., Abe, M., Ihde, J., Jentzsch, G., Naujoks, M., Wilmes, H. & Wziontek, H., 2009. Gravity field variations from superconducting gravimeters for GRACE validation, *J. Geodyn.,* **48**(3–5), 325–330, doi:10.1016/j.jog.2009.09.034.

Wenzel, H.-G., 1993. Program package GRAVNA: adjustment of gravity observations, *Fortran-program, Geodetic Institute, University Karlsruhe*, unpublished.

Zerbini, S., Richter, B., Negusini, M., Romagnoli, C., Simon, D., Domenichini, F. & Schwahn, W., 2001. Height and gravity variations by continuous GPS, gravity and environmental parameter observations in the southern Po Plain, near Bologna, Italy, *Earth planet. Sci. Lett.,* **192**(3), 267–279, doi:10.1016/S0012-821X(01)00445-9.